

Quantum transport and spin dynamics on shearless tori

K. Kudo^{1, 2, *} and T. S. Monteiro²

¹Department of Applied Physics, Graduate School of Engineering, Osaka City University, Osaka 558-8585, Japan

²Department of Physics and Astronomy, University College London,
Gower Street, London WC1E 6BT, United Kingdom

(Dated: June 7, 2008)

We investigate quantum dynamics in phase-space regions containing “shearless tori”. We show that the properties of these peculiar classical phase-space structures — important to the dynamics of tokamaks — may be exploited for quantum information applications. In particular we show that shearless tori permit the non-dispersive transmission of localized wavepackets. The quantum many-body Hamiltonian of a Heisenberg ferromagnetic spin chain, subjected to an oscillating magnetic field, can be reduced to a classical one-body “image” dynamical system which is the well-studied Harper map. The Harper map belongs to a class of Hamiltonian systems (non-twist maps) which contain shearless tori. We show that a variant with sinusoidal time driving “driven Harper model” produces shearless tori which are especially suitable for quantum state transfer. The behavior of the concurrence is investigated as an example.

PACS numbers: 75.10.Pq, 03.67.Mn, 05.45.Mt

For a Hamiltonian system, the onset of classical chaotic dynamics is associated with the disappearance of phase-space barriers termed invariant tori: when the last invariant torus disappears, the chaotic diffusive motion is unbounded (“global”). For a wide class of classical dynamical systems, described by so-called “twist-maps” and exemplified by the all-important Standard Map [1], there is a single threshold for this process, i.e., once the last invariant torus breaks, the dynamics is globally diffusive for all parameters above the threshold. However, for another class of dynamical systems described by “non-twist maps”, this is not generally the case. A new class of tori, termed “shearless tori” [2] can be present. The *classical* properties of these shearless tori are attracting considerable attention, due in part to their possible relevance to improved confinement of fusion plasmas in tokamaks [3], but also because the properties of non-twist maps are less well studied. New dynamical phenomena such as separatrix reconnection lead to the intermittent re-appearance of the shearless tori which, when present, separate different regions of the chaotic phase space.

In a quite different context, studies of quantum dynamics of spin chains, for example of quantum state transfer and entanglement generation, now play a central role in the burgeoning field of quantum information [4]. There is also growing interest in potential applications of nonlinear dynamics in quantum information. In particular, the realization that a many-body Hamiltonian can be analyzed with the dynamics of “one-body image” quantum and classical Hamiltonians [5, 6] has proved very insightful. For example, the Heisenberg ferromagnetic spin chain, in a pulsed parabolic magnetic field, has the

Standard Map as its classical image [6], provided *position* coordinates in the many-body Hamiltonian are mapped onto *momenta* of the image system and vice-versa. If, instead, a pulsed sinusoidal external magnetic field is applied and the canonical coordinates are not interchanged, the spin system maps rather onto one of the best-known non-twist maps: the kicked Harper map. The quantum dynamics of the kicked Harper map have already formed the subject of several studies [7, 8]. From the viewpoint of entanglement screening, recently, calculation of the concurrence showed that nonlinear resonances in a classically mixed phase space induce robust entangled states [9].

However, to date, the quantum dynamics near shearless tori, and their potential for quantum information applications have never been investigated. In the present study, we have calculated quantum transport along shearless tori and found it to be quite different from the dynamics along ordinary tori. In particular, we find that shearless tori provide non-dispersive transport, while ordinary tori are dispersive. In other words, for a spin chain, a spin wavepacket initially localized with starting conditions close to an ordinary torus, will rapidly become completely delocalized along the whole length of the spin chain. In contrast, for starting conditions near a shearless torus, an initially localized Gaussian wavepacket largely preserves its shape for long times, but moves along the spin chain at a near constant rate. In the chaotic regime, the shearless tori provide isolated regular ‘channels’ through the chaotic sea which can be used to propagate coherent spin states (approximately) non-dispersively. We show that, for a driven Harper model, one may even start the wavepacket with zero momentum. We attribute the non-spreading of quantum wavepackets near shearless tori to a local quasienergy spectrum (i.e., for the Floquet states localized on the shearless tori) which is a perturbed harmonic spectrum. The corresponding evolution of the concurrence was also obtained.

We consider the Heisenberg ferromagnetic spin chain

*Electronic address: kudo.kazue@ocha.ac.jp; Present address: Ochadai Academic Production, Ochanomizu University, 2-1-1 Ohtsuka, Bunkyo-ku, Tokyo 112-8610, Japan

under an oscillating magnetic field. Here, we concentrate on a spin-1/2 and one-down-spin case, where a state is in a superposition of the states where one spin is down and the others are up. In that case, the model corresponds to a tight-binding model with an oscillating field of amplitude B_0 by the Jordan-Wigner transformation. Since the total S_z is conserved, i.e. the one-down-spin state is conserved, the correlation terms disappear. Then, the Hamiltonian is written as

$$H(t) = \frac{J}{2} \sum_{j=1}^N (c_j^\dagger c_{j+1} + c_{j+1}^\dagger c_j) + B_0 F(t) \sum_{j=1}^N \cos\left(\frac{2\pi}{N}j\right) c_j^\dagger c_j. \quad (1)$$

Here, c_j^\dagger and c_j are the creation and annihilation operators of a fermion at the j th site, respectively. For ferromagnetic cases, $J < 0$. The total number of sites is N , and periodic boundary conditions are imposed. $F(t)$ is a periodic function of time with period T .

We solve spin dynamics from Eq. (1). However, to analyze the quantum behavior, we first note this: In the absence of the time-dependent external field, the model (1) is associated with a dispersion relation, obtained from the Bethe ansatz, $E_i = J(1 - \cos k_i)$ with $i = 0, 1, 2, \dots, N$ and where the E_i are energy eigenvalues and the k_i quantized wavenumbers. Equating the k_i with the momenta of a classical system [5, 6], i.e., $k_i \rightarrow p$ and taking a continuous position variable $x_j = \frac{2\pi}{N}j \rightarrow \frac{2\pi}{N}x$, we can see that Eq. (1) maps onto the one-body classical “image” Hamiltonian:

$$H(x, p, t) = J \cos p + B_0 F(t) \cos[(2\pi/N)x]. \quad (2)$$

If $F(t) = \sum_n \delta(t - nT)$, we have the usual kicked Harper model. Here, we take $F(t) = \sin \omega t$, with $\omega = 2\pi/T$, and investigate a modification we term the “driven-Harper model”. The corresponding classical equations of motion are given by:

$$\begin{cases} \dot{x} = -J \sin p & (0 < x \leq N), \\ \dot{p} = (2\pi/N)B_0 \sin \omega t \sin[(2\pi/N)x] & (-\pi < p \leq \pi). \end{cases} \quad (3)$$

Integrating Eq. (3) numerically, we obtain $x(t)$ and $p(t)$. Classical surfaces of section (SOS) are obtained by plotting values of (x, p) at integer multiples of the period, $t = n(2\pi/\omega)$, where n is an integer. Three SOS are shown in Fig. 1. Here, we set $J = -1$, $B_0 = 2$, $N = 100$, and these values are fixed below. With decreasing frequency $\omega = 0.20, 0.16, 0.12$, the classical phase space becomes increasingly chaotic; at $\omega = 0.16$ all tori have disappeared; however, at $\omega = 0.12$, shearless tori have re-appeared, embedded in two regular ‘channels’ running through a fully chaotic phase space (bar a few very small stable islands).

For the kicked Harper map, shearless tori occur for $p \approx \pm\pi/2$ [2]. They correspond to an extremum of the rotation number; here $\frac{\partial \dot{x}}{\partial p} = 0$ at $p \simeq \pm\pi$. The shearless tori for $\omega = 0.12$ are extremely distorted and span the full range of the map, from $p = 0$ to $\pm\pi/2$. The kicked

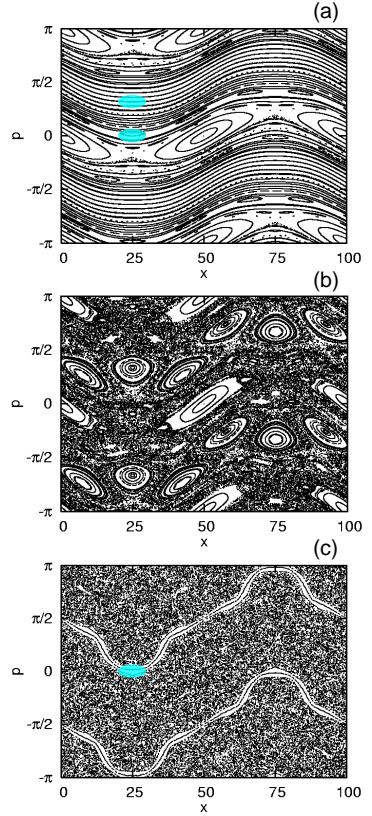


FIG. 1: (Color online) Classical phase space for (a) $\omega = 0.20$ (near integrable), (b) $\omega = 0.16$ mixed phase-space with no apparent tori, and (c) $\omega = 0.12$ showing the re-appearance of shearless tori: phase space is almost entirely chaotic but regular channels, containing shearless tori, which separate different chaotic regions, are seen. The colored patched areas correspond to the initial wave packet of quantum dynamics in Fig. 2.

Harper map, on the other hand, does not produce shearless tori which include the $p = 0$ region, so for this reason, using a driven rather than a kicked spin chain is advantageous. In other words, to prepare a spin-wave packet on the shearless torus region, one should excite low energy $E(k_j) \simeq 0$ spin-waves (i.e., $k_j \simeq 0$ since this corresponds to the bottom of the $E(k_j)$ energy band) in the region of the spin chain containing a node of the magnetic field (i.e., $x_j \approx \pi/2$ or $x_j \approx 3\pi/2$). Exciting low-energy spin waves is a simpler procedure than selecting a more precise range of higher-energies, which would be required if the shearless tori are only found at $p \approx \pi/2$ as is the case for the kicked system.

Returning now to our spin-Hamiltonian, Eq. (1), we compare the time evolution of a spin wavepacket with initial conditions corresponding, in the image classical system, to shearless tori with those of normal tori. We consider the quantum spin distribution:

$$P(j, t) = |\langle j | \psi(t) \rangle|^2. \quad (4)$$

where $|j\rangle$ is the state where the j th spin is down, and

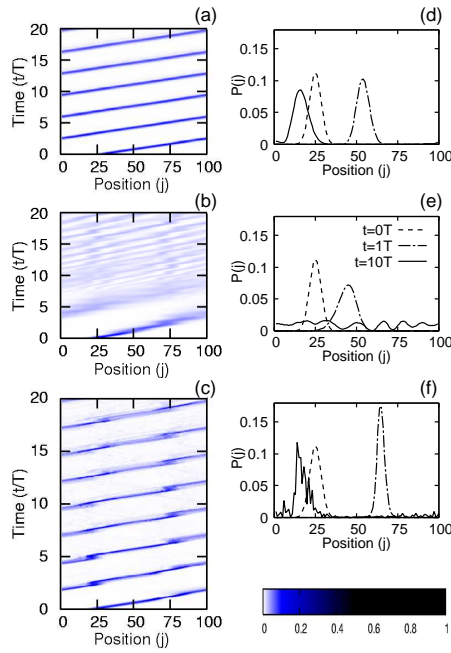


FIG. 2: (Color online) Time evolution of a quantum spin-wavepacket, initially centered at $j_0 = 25$, showing dispersive propagation on normal tori and non-dispersive propagation on shearless tori. (a) $\omega = 0.20$ and $k_0 = 1.0$; wavepacket prepared initially on shearless torus of Fig. 1(a), but in the near integrable regime. (b) $\omega = 0.20$ and $k_0 = 0.0$; initial state is on an ordinary torus of Fig. 1(a) and rapidly delocalizes along the length of the spin-chain. (c) $\omega = 0.12$ and $k_0 = 0.0$; the spin wavepacket initially on shearless torus embedded in the chaotic sea of Fig. 1(c) propagates largely without dispersion, but the effect is less pronounced than in the integrable case. (d), (e), and (f) correspond to (a), (b), and (c), respectively. They exhibit the form of wavepackets after $t = 0T$, $1T$, and $10T$.

$|\psi(t)\rangle$ is calculated from Eq. (1). Our initial state $|\psi(t=0)\rangle$ is a Gaussian spin wavepacket with the phase space area corresponding to the classical plot in Fig. 1. The center of the wavepacket is denoted by j_0 and k_0 in the real and momentum space, respectively. The width of the wavepacket is set to be $\Delta_j = 5$.

In Fig. 2(a), we show the behavior (for $\omega = 0.20$) of a wavepacket initially centered on $j_0 = 25$ and $k_0 = 1.0$ (i.e., mapping onto a regular phase-space region in the image classical system including a shearless torus). the distribution shows very little delocalization for as long as the numerics were run (20 periods). Despite the same frequency, the distribution in Fig. 2(b), which initially centered on the region corresponding to normal tori in the classical map, rapidly delocalizes and there is no discernible localization at $t = 10T$. However, Fig. 2(c) (for $\omega = 0.12$) shows again little delocalization of the wavepacket initially centered on $j_0 = 25$ and $k_0 = 0.0$ (i.e., on a shearless torus). Numerical experiments show that an equivalent classical ensemble of particles around a shearless torus spread slowly: the lack of shear also

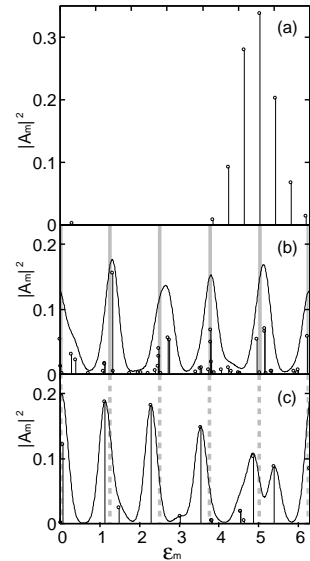


FIG. 3: Quasi-energy spectrum local to shearless tori, showing that it corresponds to a near harmonic spectrum in the near-integrable limit and a perturbed harmonic spectrum in the chaotic limit. The spectrum is plotted for $|A_m|^2 > 10^{-3}$. The low resolution spectrum is a Gaussian-smoothed one. The gray broad bars are just an eye guide, and their interval is $2\pi/5$. (a) Quasienergy spectrum for $\omega = 1.0$ showing equal quasi-energy spacing. (b) Low resolution (smoothed) spectrum near shearless tori embedded in chaotic sea for $\omega = 0.12$ showing the spectrum approximates a perturbed harmonic spectrum. (c) Low resolution spectrum near ordinary torus at $\omega = 0.20$.

produces a strong classical effect.

One can attempt to understand the quantum behavior from its quasi-energy spectrum: as this is a temporally periodic system, it is the eigenstates of the one-period unitary evolution operator (Floquet states) $\phi_m(x, t)$ and associated eigenphases (quasi-energies) ε_m which represent the stationary states of the system. One should first emphasize that the non-dispersive behavior is not simply a wavepacket revival effect [10] where a wavepacket may partially or totally regain its shape after some revival time, dependent on the underlying frequencies. In our case, the wavepacket does not ever lose its essential shape. The behavior is rather analogous to motion of a wavepacket on a harmonic potential: the wavepacket oscillates in position without spreading; if the shape of the underlying potential is different (so our Δ_j is not the width of its ground state) the wavepacket exhibits only a certain ‘breathing’ in its width, demonstrated in [10]. The modest variability in the wavepacket shape seen in Fig. 2 would be compatible with such breathing.

We have calculated the local Floquet spectrum for the initial Gaussian wavepacket, i.e., the overlap between the wavepacket and the Floquet states, $A_m = \langle \phi_m(x, t = 0) | \psi_0 \rangle$. The probability $|A_m|^2$ is plotted in Fig. 3 as a function of quasi-energy. For the wavepacket on a shearless torus in a near-integrable regime, shown in Fig. 3(a),

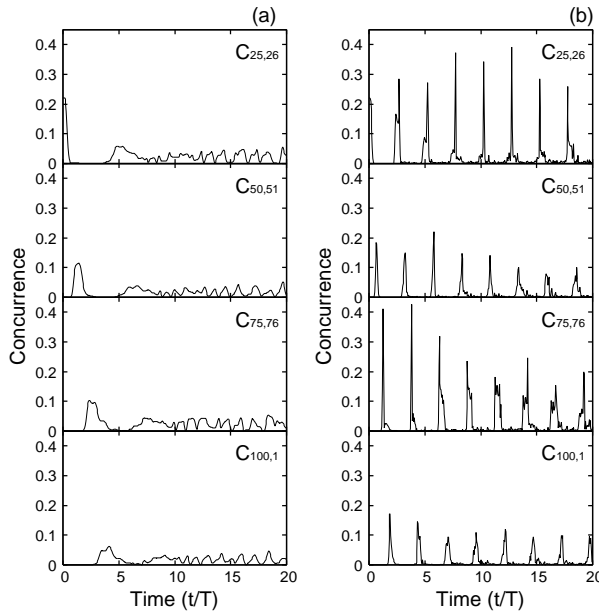


FIG. 4: Time evolution of the concurrence, contrasting entanglement transport by wavepackets moving along normal tori (left panels) with the non-dispersive shearless tori (right panels). (a) $\omega = 0.20$ showing broad small peaks corresponding to Fig. 2(b), and (b) $\omega = 0.12$ showing periodic sharp peaks corresponding to Fig. 2(c).

a ‘harmonic’ ladder of equally-spaced eigenstates is evident. In Fig. 3(b), the shearless torus embedded in the chaotic regime, the low-resolution smoothed spectrum shows a set of equally spaced peaks. The interval of the peaks is $2\pi/5$. This corresponds to the fact that the wave packet returns almost the same position as the initial one after 5 cycles ($t = 5T$). We propose that this represents a perturbed harmonic spectrum found for eigenstates local to shearless tori, in the near-integrable regime. In the chaotic regime [Fig. 3(b)], the eigenstates are no longer completely localized on the shearless torus region and overlap with the chaotic regions; conversely, eigenstates

with most support from the chaotic regions overlap with the torus region. Consequently, the states no longer form a ladder of individual states, but their amplitude is split redistributed into a cluster of nearby states. Nevertheless, the presence of these regularly spaced clusters is sufficient to hinder dispersion of the wavepacket for a considerable time. For the ordinary torus, however, the spacing is irregular and even with smoothing, and the low-resolution spectrum has no equal spacing as shown in Fig. 3(c).

The entanglement is also transported when the Gaussian packet travels. We employ the concurrence $C_{i,j}$, which is a measure of the bipartite entanglement of two sites i and j [11]. We concentrate on the cases corresponding to Figs. 2(b) and 2(c) as we are interested in the transport of quantum information. Figure 4 shows the time evolution of the concurrence, $C_{25,26}$, $C_{50,51}$, $C_{75,76}$, and $C_{100,1}$ for (a) $\omega = 0.20$ and (b) $\omega = 0.12$. Here, we should notice that the 100th and 1st sites are neighboring sites because of the periodic boundary conditions. In Fig. 4(a), no sharp peaks appear, although we can see some small peaks. On the other hand, in Fig. 4(b), the concurrence has sharp periodic peaks. Moreover, several peaks are much higher than the initial value, $C_{25,26}(t = 0) \simeq 0.22$. This behavior of the concurrence corresponds closely to that seen in the spin dynamics.

In conclusion, we find that quantum transport using shearless tori has a very different character from that associated with normal tori. The quantum spin chain under an oscillating field can, for certain conditions, provide approximately non-dispersive transport even in a largely chaotic regime. The non-dispersion of Gaussian states is a property associated with large stable islands, in fact. These have been shown recently to preserve entanglement against noise [9]. The shearless tori may well provide a similar advantage while also transporting entanglement around the spin chain.

The authors thank K. Nakamura and S. Bose for helpful discussions and K.K. thanks the JSPS for support.

[1] E. Ott, *Chaos in dynamical systems*, Cambridge University Press (2005).

[2] S. Shinohara and Y. Aizawa, *Prog. Theor. Phys.* **97**, 379 (1997); S. Shinohara and Y. Aizawa, *Prog. Theor. Phys.* **100**, 219 (1998); S. Shinohara, *Phys. Lett. A* **298**, 330 (2002).

[3] P. Morrison, *Phys. Plasmas*, **7** 2279 (2000); F.M. Levinton *et al.*, *Phys. Rev. Lett.* **75**, 4417 (1995); J.S.E. Portela, I.L. Caldas, R.L. Viana and P.J. Morrison, *Int. J. Bifurcation and chaos*, **17**, 1589 (2007).

[4] S. Bose, *Phys. Rev. Lett.*, **91** 207901 (2003); L. Amico, R. Fazio, A. Osterloh and V. Vedral, *quant-ph/0703044* (2007).

[5] T. Prosen, *Phys. Rev. Lett.*, **80** 1808 (1998); T. Prosen, *Phys. Rev. E* **60**, 1658 (1999); T. Prosen, *Phys. Rev. E* **65**, 036208 (2002).

[6] T. Boness, S. Bose, and T.S. Monteiro, *Phys. Rev. Lett.* **96**, 187201 (2006).

[7] R. Lima and D. Shepelyansky, *Phys. Rev. Lett.* **67**, 1377 (1991); T. Geisel, R. Ketzmerick, and G. Petschel, *Phys. Rev. Lett.* **66**, 1651 (1991); I.I. Satija and B. Sundaram, *Phys. Rev. Lett.* **84**, 4581 (2000); R. Artuso and L. Rebuzzini, *Phys. Rev. E* **66**, 017203 (2002); J. Gong and P. Brumer, *Phys. Rev. Lett.* **97**, 240602 (2006).

[8] I. Dana, *Phys. Lett. A* **197**, 413 (1995); I. Dana, *Phys. Rev. E* **52**, 466 (1995); I. Dana and D.L. Dorofeev, *Phys. Rev. E* **72**, 046205 (2005).

[9] I. García-Mata, A.R.R. Carvalho, F. Mintert, and A. Buchleitner, *Phys. Rev. Lett.* **98**, 120504 (2007).

[10] B.M. Garraway and Kalle-Antti Suominen, *Rep. Prog. Phys.*

Phys. **58** 365 (1995).
[11] W.K. Wootters, Phys. Rev. Lett. **80**, 2245 (1998).